Satellite detection of soil moisture impacts on convection at the mesoscale

Christopher M. Taylor, Richard J. Ellis

Centre for Ecology and Hydrology, Wallingford, United Kingdom.

An edited version of this paper was published by AGU. Copyright 2006 American Geophysical Union. Taylor, C. M., and R. J. Ellis (2006), Satellite detection of soil moisture impacts on convection at the mesoscale, Geophys. Res. Lett., 33, L03404, doi:10.1029/2005GL025252.

Understanding of interactions between soil moisture and precipitation is limited by a lack of direct observations at spatial scales on which feedbacks occur. This study identifies a sensitivity of convective cloud to spatial variations in soil moisture, based on analysis of satellite observations from many cases in the Sahel. Patches of wet soil were located using passive microwave data. The patches were composited according to length scale, ranging from 37 to 200 km. The response of the convective cloud field to surface variability along the composite cross-section was studied with thermal infra-red data. A suppression of convective cloud is evident over the wet soil during the afternoon and evening for all but the smallest length scales. Analysis of over 100 individual cases where convection occurred in the vicinity of a patch revealed that the development of cloud systems in their early stages appears to be particularly sensitive to soil moisture.

1. Introduction

Soil moisture can play an important role in influencing surface fluxes, the planetary boundary layer, and the development of moist convection [e.g. *Betts and Ball*, 1998]. Much of our knowledge concerning the coupling between soil moisture and precipitation has been gleaned from numerical models. However, as shown rather dramatically by *Koster et al.* [2004], different atmospheric models have contrasting sensitivities to the land surface.

To gain insight into how the coupled system functions, and to better constrain our models, observations are a valuable tool. Monitoring soil moisture on length scales likely to affect moist convection (upwards of a few kilometres) requires the use of satellite data. One of the most promising approaches is the use of passive microwave to detect variations in moisture in the top few centimetres of the soil [e.g. *Jackson*, 1993]. For understanding land-atmosphere coupling, this method is particularly appealing in regions where the vegetation cover is sparse (dense vegetation attenuates the soil moisture signal), and the partition between surface sensible and latent heat is rather sensitive to near surface soil moisture. In this study, horizontal variations in soil moisture are detected using microwave data, and the influence of the variability on the atmosphere is assessed using Thermal Infra-Red (TIR) imagery from Meteosat.

2. TRMM Data Processing

Measurements of horizontally and vertically polarised brightness temperature at 10.65 GHz from the Tropical Rainfall Measuring Mission (TRMM) Microwave Imager are exploited here. TRMM data have been used by, amongst others, *Bindlish et al.* [2003] to make quantitative estimates of soil moisture. We use time series of the polarisation ratio in the West African Sahel to locate areas of increased soil moisture. An example of a time series from a region in Niger covering

approximately 2000 km^2 is presented in Figure 1. Based on satellite measurements available typically once per day, the figure shows low values of polarisation ratio in the aftermath of rainfall, followed over several days without further storms, by relaxation back to a characteristic "dry" value. A lower frequency signal (an increase during the wet season) is associated with longer time scale changes in the land surface, notably the development of a vegetation layer. The solid line in the figure represents the low frequency changes in polarisation when the soil surface is assumed to be dry. These values are computed by first interpolating pixel values onto a regular grid, then by linearly interpolating in time the maximum polarisation ratio occurring within a moving window of 21 days. In this paper, daily anomalies in polarisation ratio (Δ_{pr}) are calculated relative to the low frequency "dry" signal.

Data from TRMM were analysed for a single wet season (June to September 2000) over a region stretching from 10ºN to 20ºN, and between the Atlantic coast (around 16ºW) and 15ºE. This region is relatively flat, and is dominated by a strong meridional gradient in rainfall, with the vegetation becoming increasingly sparse moving northwards. To illustrate typical spatial patterns of soil wetness detected by TRMM, Figure 2 presents data from two orbits on the evening of August 3 2000. Values of Δ_{pr} are shown for each pixel in the orbit, based on deviations of the polarisation ratio from the "dry" value on that day, interpolated to the pixel locations. Areas of significant topography and water bodies are excluded, as are pixels affected by current rainfall based on an algorithm presented by *Ferraro et al.* [1998]. The figure highlights two distinct large-scale wet areas (labelled *A* and *B*). These correspond to areas of cold cloud detected using TIR imagery from the previous 15 hours. Wet patch *A* illustrates the characteristic surface rainfall signature of a Sahelian Mesoscale Convective System (MCS), travelling approximately 1000 km in a roughly south-westerly direction.

To produce robust results based on a large number of cases, a composite approach was adopted. Sections across wet patches of different sizes were combined from data throughout the domain and season. To maintain the highest possible spatial resolution, the cross-sections followed individual scan lines, which arc across the swath (as shown over patch *A* in Figure 2). Values of Δ_{pr} were averaged over 4 adjacent pixels along the scan to provide data at the resolution of the sensor (approximately 37 km [*Kummerow et al.*, 1998]). Wet strips were identified when the 4-pixel average value of Δ_{pr} over some length scale (L) fell below -0.03 whilst values from the adjacent pixels (within L/2 of the strip) remained above -0.015. An example of one such strip is shown in Figure 2. The crosses mark the bounds of the wet strip on the scan line, which in this case was of length 18 pixels. In the compositing of such soil moisture patterns, a maximum of one strip in every 3 scans (approximately 42 km) was used to limit the effect of sampling the same 2 dimensional patch many times. The resulting composites were made up of 1559 cases of length scales 4 to 22 pixels (37 to 200 km). These cases were distributed fairly regularly in time and space. This ensured that individual cases could not dominate the composite.

3. Cold cloud field around composite wet strip

Hourly Meteosat TIR data were used to assess the evolution of deep convective cloud along TRMM scan lines containing wet strips. Each TRMM pixel contains typically 4 or 5 Meteosat pixels. For every TRMM pixel in the composite, the percentage coverage of Meteosat pixels colder than a threshold of -40ºC was computed. This calculation was performed for a period of 72 hours starting at 0600 UTC on the morning following the TRMM overpass. Figure 3 presents the results of this analysis for the 739 strips of between 8 and 20 pixels (74 and 185 km) for the first 30 hours. At all locations along the composite cross-section, there is a strong daytime minimum in cold cloud, typical of the region [e.g. *Mathon et al.*, 2002] with increases in late afternoon and early evening.

There also tends to be more cold cloud in the right of the composite. This is because on average, the right hand side samples more southerly pixels, and is therefore climatologically cloudier. The effect of the wet patch can be seen by the reduced cloud in the afternoon and evening over wet soils compared to adjacent drier regions. Between 1700 and 2000 UTC when mean convection is increasing rapidly, at the centre of the wet anomaly the effect is equivalent to a 37% reduction in cloudiness compared to the values at the left and right hand sides of the figure. A weaker reduction in cloudiness over the wet strip is apparent on the evening of day 2 (not shown), after which the signal disappears. It should be noted that the cloud systems associated with the early evening signal in Figure 3 are independent of the storms which produced the original soil moisture anomaly, and which typically occurred the previous day. Rather, the evolution of the composite cloud field is consistent with a negative feedback between soil moisture and convection. Wet soils tend to be associated with less subsequent cold cloud and (assuming that cold cloud is a reasonable proxy for precipitation) less rainfall. As the initial wet patch dries, typically over 1 or 2 days [e.g. *Gash et al.*, 1997], and subsequent rain events occur, the surface fluxes in the composite should become less coherent in space, and therefore have a weaker impact on the composite cloud field.

Figure 4 presents an analysis of evening cloudiness as a function of surface length scale. For a wet strip of 4 pixels (37 km) there is no discernible impact of soil moisture on variability of cloud in the region between 1700 and 2000. Only the large-scale gradient (increasing left to right) is apparent. For all the remaining length scales examined, cloudiness is reduced over the wet strip compared to the adjacent drier regions, consistent with a negative feedback. Convective cloud is an inherently noisy field, and this means that it is not possible to draw statistically significant conclusions about the relative strengths of the feedback at length scales larger than 4 pixels from a data set of this size.

4. Examination of individual cases

An impact of soil moisture on cloudiness can be identified from Fig. 3 during certain phases of the diurnal and soil drying cycle. However, the composite provides little evidence about the atmospheric processes involved. We therefore examined individually 108 different patches from the composite where cold cloud was detected between 1700 and 2000 UTC. For each case, time series of Meteosat imagery were analysed to locate the initiation of the cloud system, the characteristics of the system upstream of the patch, and its evolution as it passed over the wet patch. An example of one such case is presented in Figure 5. In this case, data from a TRMM orbit at 2215 UTC on 12 June highlight distinct wet areas associated with cold cloud from that morning. On the following afternoon (13 June), convection was initiated in 3 locations (X, Y and Z). These systems expanded and propagated towards the south-west. However, system Y moved to the north-west rather than pass over the wettest soil, whilst the latitudinal expansions of systems X and Z were halted at the edges of wet areas.

The single case presented in Figure 5 suggests that the development of the convective systems was strongly influenced by the soil moisture field. Based on similar visual analysis of the 107 other cases, some firmer conclusions can be drawn concerning the origins of the composite mean pattern (Figure 3). In only 2 of the 108 cases was a convective system initiated over wet soil. In 58 cases (54%), cold cloud cover decayed sharply moving across dry-wet transitions, as in Figure 5. In 28 cases (26%), the cloud pattern bore no discernible similarity to the soil moisture, whilst the remaining 22 cases did not fall conclusively into either of these categories. Further analysis based on how far upstream the systems initiated provided additional insight. Of the 39 systems initiated within 100 km of the patch, 34 (87%) exhibited less cloud over the wet patch than the surroundings. Systems initiated further upstream tended to be much larger by the time they reached the wet patch

and showed a markedly lower apparent sensitivity to the wet patch, with only 51% of cases illustrating cloud gradients located above soil moisture transitions. Overall, this analysis suggests that the relatively weak storm activity apparent in Fig. 3 over the wet strip is linked to the initiation and passage of small convective systems (typically less than 200 km across). Possible physical mechanisms to explain this finding are discussed below.

5. Discussion

The data presented here show marked suppression of cold cloud during the afternoon and evening over wet soils as compared to adjacent drier areas. This signal is associated with suppressed convective initiation over wet soils. There is a tendency in the dataset for small-scale convective systems to propagate over dry soils, whilst larger systems appear less sensitive. The implied negative feedback between soil moisture and precipitation contrasts with the results of *Taylor and Lebel* [1998] from this region, who proposed a positive feedback mechanism operating at scales ~ 10 – 15 km to explain observed persistent rainfall patterns.

A possible explanation lies in the thermodynamics of convective initiation. Surface fluxes from wet soils produce shallower, moister and cooler boundary layers compared to drier soils. However, the sensitivity of convective initiation to soil moisture depends not only on surface processes. The stability of the layer into which the boundary layer is growing is considered to be important for determining the sign of a feedback [*Ek and Mahrt*, 1994]. *Findell and Eltahir* [2003] argue that if the temperature profile between 900 and 700 hPa is close to dry adiabatic then the triggering of moist convection is more likely when soils are dry. This is the case in the Sahel, where the deep, well-mixed Saharan air layer overlies a shallow moist adiabatic monsoon layer [*Parker et al.*, 2005]. Thus one might expect convective initiation to occur preferentially over dry soils - a negative feedback.

However, about 90% of the rainfall in the Sahel is produced by long-lived and well-organised MCS [*Mathon et al.*, 2002], and the physics of a soil moisture feedback may differ here from the convective initiation case. Organised MCS are associated with a strong cold pool that forces ascent, and rainfall is sensitive to convective available potential energy (CAPE). Dry soils produce lower CAPE than wet soils, and a positive feedback from MCS (as inferred by *Taylor and Lebel* [1998]) may be favoured. In the present study, the negative feedback is strongest during the late afternoon and early evening, when convective systems tend to be small [*Mathon et al.*, 2002], and is indeed relatively weak for longer-lived systems.

Other satellite studies looking at the impact of land cover variability on cloudiness have also found suppression of afternoon convection over relatively freely evaporating surfaces [*Carleton et al.*, 2001; *Negri et al.*, 2004; *Rabin et al.*, 1990]. The former two studies both hypothesised a key role for the pre-storm dynamical response of the atmosphere to the surface forcing. Strong horizontal gradients in sensible heat flux can generate sea breeze type circulations in the lower atmosphere. From modelling studies [e.g. *Avissar and Liu*, 1996] the mesoscale updrafts of such circulations could provide the focus for moist convection. In the context of this study, one would expect afternoon convective initiation to occur preferentially over dry soils adjacent to the wet patch, with a strong dependency on patch length scale, as found here. Such circulations are rather sensitive to the large-scale wind conditions, a characteristic that we were unable to isolate in this dataset using wind data from atmospheric analyses. A better understanding of the role of such processes in surface – atmosphere feedbacks will certainly emerge from the forthcoming African Monsoon Multidisciplinary Analyses (AMMA) campaign in the summer of 2006.

Acknowledgements

This work was funded by the NERC through the CLASSIC Centre NER/P/S/2002/00205, and by the European Union Framework 6 Integrated Project, AMMA-EU. The TRMM data were made available through the Goddard Distributed Active Archive Center, and the Meteosat data provided by EUMETSAT. We would like to thank the anonymous reviewers for their helpful comments on the text.

References

Avissar, R., and Y. Q. Liu (1996), 3-dimensional numerical study of shallow convective clouds and precipitation induced by land-surface forcing, *J. Geophys. Res. - Atmospheres*, *101*, 7499-7518.

Betts, A. K., and J. H. Ball (1998), FIFE surface climate and site-average dataset 1987-89, *J. Atmos. Sci.*, *55*, 1091-1108.

Bindlish, R., T. J. Jackson, E. Wood, H. L. Gao, P. Starks, D. Bosch, and V. Lakshmi (2003), Soil moisture estimates from TRMM Microwave Imager observations over the Southern United States, *Remote Sens. Environ.*, *85*, 507-515.

Carleton, A. M., J. Adegoke, J. Allard, D. L. Arnold, and D. J. Travis (2001), Summer season land cover - convective cloud associations for the Midwest US "Corn Belt", *Geophys. Res. Lett.*, *28*, 1679-1682.

Ek, M., and L. Mahrt (1994), Daytime evolution of relative humidity at the boundary layer top, *Mon. Weather Rev.*, *122*, 2709-2721.

Ferraro, R. R., E. A. Smith, W. Berg, and G. J. Huffman (1998), A screening methodology for passive microwave precipitation retrieval algorithms, *J. Atmos. Sci.*, *55*, 1583-1600.

Findell, K. L., and E. A. B. Eltahir (2003), Atmospheric controls on soil moisture-boundary layer interactions. Part I: Framework development, *J. Hydromet.*, *4*, 552-569.

Gash, J. H. C., P. Kabat, B. A. Monteny, M. Amadou, P. Bessemoulin, H. Billing, E. M. Blyth, H. A. R. de Bruin, J. A. Elbers, T. Friborg, G. Harrison, C. J. Holwill, C. R. Lloyd, J. P. Lhomme, J. B. Moncrieff, D. Puech, H. Soegaard, J. D. Taupin, A. Tuzet, and A. Verhoef (1997), The variability of evaporation during the HAPEX-Sahel intensive observation period, *J. Hydrol.*, *189*, 385-399.

Jackson, T. J. (1993), Measuring Surface Soil-Moisture Using Passive Microwave Remote-Sensing .3, *Hydrol. Proc.*, *7*, 139-152.

Koster, R. D., P. A. Dirmeyer, Z. C. Guo, G. Bonan, E. Chan, P. Cox, C. T. Gordon, S. Kanae, E. Kowalczyk, D. Lawrence, P. Liu, C. H. Lu, S. Malyshev, B. McAvaney, K. Mitchell, D. Mocko, T. Oki, K. Oleson, A. Pitman, Y. C. Sud, C. M. Taylor, D. Verseghy, R. Vasic, Y. K. Xue, and T. Yamada (2004), Regions of strong coupling between soil moisture and precipitation, *Science*, *305*, 1138-1140.

Kummerow, C., W. Barnes, T. Kozu, J. Shiue, and J. Simpson (1998), The Tropical Rainfall Measuring Mission (TRMM) sensor package, *J. Atmos. Oceanic Technol.*, *15*, 809-817.

Mathon, V., H. Laurent, and T. Lebel (2002), Mesoscale convective system rainfall in the Sahel, *J. Appl. Meteorol.*, *41*, 1081-1092.

Negri, A. J., R. F. Adler, L. M. Xu, and J. Surratt (2004), The impact of Amazonian deforestation on dry season rainfall, *J. Climate 17*, 1306-1319.

Parker, D. J., C. D. Thorncroft, R. R. Burton, and A. Diongue-Niang (2005), Analysis of the African easterly jet, using aircraft observations from the JET2000 experiment, *Q. J. R. Meteorol. Soc.*, *131*, 1461-1482.

Rabin, R. M., S. Stadler, P. J. Wetzel, D. J. Stensrud, and M. Gregory (1990), Observed effects of landscape variability on convective clouds, *Bull. Am. Meteorol. Soc.*, *71*, 272-280.

Taylor, C. M., and T. Lebel (1998), Observational evidence of persistent convective-scale rainfall patterns, *Mon. Weather Rev.*, *126*, 1597-1607.

Figures

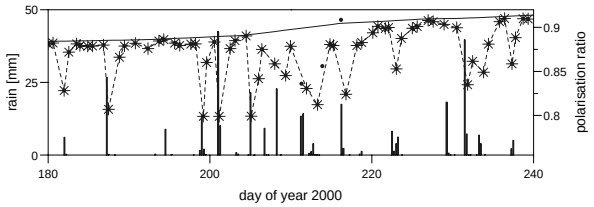

Figure 1. Time series of polarisation ratio data (asterisks) averaged over 13.5-13.9ºN, 2.4-2.8ºW. The solid line indicates the daily values of the assumed "dry" ratio, based on the maximum ratio measured within a 21 day running mean. Note that additional data points where measurements from only part of the region are available are also plotted (circles). These can influence the full area-average dry values, notably on day 216. Also plotted (bars) are 6 hourly rainfall totals averaged over 9 gauges within this area. (Rainfall data courtesy of Thierry Lebel, IRD).

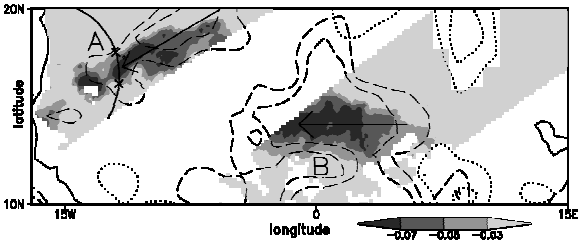

Figure 2. Satellite data from 3 August (day 216). Shaded contours denote values of Δ_{pr} from TRMM overpasses at 1945 and 2115 UTC. The dashed contour lines indicate mean antecedent cold cloud coverage of 10% and 20% during the period 0600-2200 UTC. The direction of travel of the cloud systems is shown by the arrows. Dotted contours mark topographic height exceeding 500 and 750 m. A single scan line is drawn over wet patch A, the two crosses marking the edges of a wet strip used in the composite.

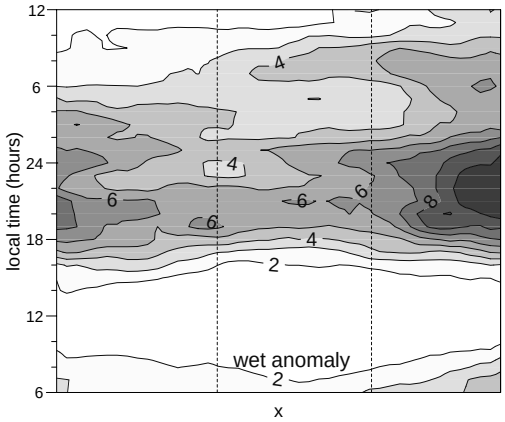

Figure 3. Evolution of composite cold cloud cover [%], along the patch cross-section (x). The data from strips of different length scales have been normalised so that the wet pixels lie within the dashed vertical lines.

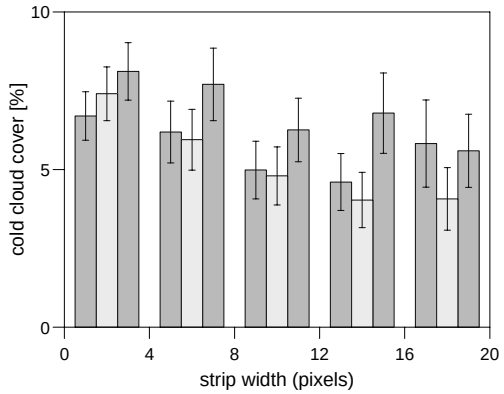

Figure 4. Composite cold cloud cover [%] averaged over the wet strip (pale bar) and adjacent pixels (dark bars) between 1700 and 2000 UTC as a function of strip length scale. The line bars indicate the standard error of the composite mean value.

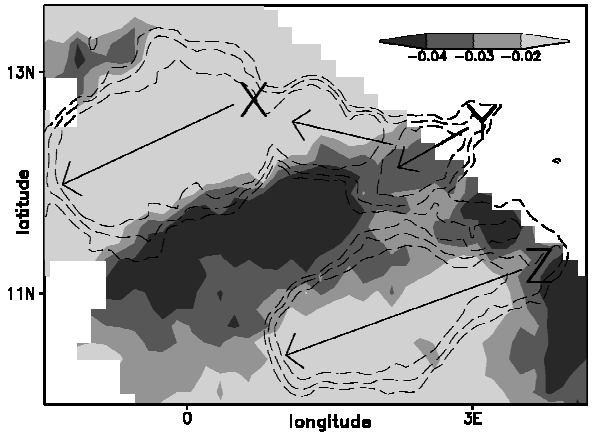

Figure 5. Minimum TIR temperatures (contours at -20, -40 and -60ºC) detected by Meteosat between 1500 and 2100 UTC on 13 June in the region of a wet patch identified by low (dark) values of Δ_{pr}. Initiation of 3 distinct systems occurred at X, Y and Z, and the direction of their propagation is denoted by the arrows.